FSU-HEP-2009-0314
UCLA/09/TEP/49

W- and Z-boson production with a massive bottom-quark pair at the Large Hadron Collider

F. Febres Cordero*

Department of Physics and Astronomy,

UCLA, Los Angeles, CA 90095-1547, USA

L. Reina†

Physics Department, Florida State University, Tallahassee, FL 32306-4350, USA

D. Wackeroth‡

Department of Physics, SUNY at Buffalo, Buffalo, NY 14260-1500, USA

(Dated: December 7, 2009)

Abstract

We present total and differential cross sections for $Wb\bar{b}$ and $Zb\bar{b}$ production at the CERN Large Hadron Collider with a center-of-mass energy of $\sqrt{s} = 14$ TeV, including Next-to-Leading Order (NLO) QCD corrections and full bottom-quark mass effects. We also provide numerical results obtained with a center-of-mass energy of $\sqrt{s} = 10$ TeV. We study the scale uncertainty of the total cross sections due to the residual renormalization- and factorization-scale dependence of the truncated perturbative series. While in the case of $Zb\bar{b}$ production the scale uncertainty of the total cross section is reduced by NLO QCD corrections, the $Wb\bar{b}$ production process at NLO in QCD still suffers from large scale uncertainties, in particular in the *inclusive* case. We also perform a detailed comparison with a calculation that considers massless bottom quarks, as implemented in the Monte Carlo program MCFM. The effects of a non-zero bottom-quark mass (m_b) cannot be neglected in phase-space regions where the relevant kinematic observable, such as the transverse momentum of the bottom quarks or the invariant mass of the bottom-quark pair, are of the order of m_b. The effects on the total production cross sections are usually smaller than the residual scale uncertainty at NLO in QCD.

*Electronic address: ffebres@physics.ucla.edu

†Electronic address: reina@hep.fsu.edu

‡Electronic address: dow@ubpheno.physics.buffalo.edu

I. INTRODUCTION

The Large Hadron Collider (LHC) at CERN (Geneva, Switzerland) is scheduled to start operation by the end of 2009. One of the most important items on its agenda is the investigation of the mechanism of electroweak symmetry breaking (EWSB), in particular the discovery of one or more Higgs bosons. Once discovered, the measurement of the Higgs bosons' properties will be crucial to unravel the underlying EWSB mechanism. The production of a weak gauge boson, $W^{\pm}$ (from now on indicated simply as W unless differently specified) or Z, with a pair of bottom (b) quarks, contributing to both the $W/Z+1\,b$-jet and $W/Z+2\,b$-jets signatures, represents both an interesting Standard Model (SM) signal and one of the most important background processes to many Higgs-boson production channels.

The cross sections for W and Z boson production with bottom quarks has been measured at the Tevatron $p\bar{p}$ collider at Fermilab ($\sqrt{s}$ = 1.96 TeV) by both the CDF [1, 2] and D0 [3, 4] collaborations. These measurements will continue with increased precision, which will provide a unique opportunity to test and improve the theoretical description of heavy-quark jets at hadron colliders by performing a thorough comparison between the Tevatron experimental data and existing theoretical predictions. Studying the same cross sections in the very different kinematic regimes available at the LHC pp collider will then be of great interest and will represent a crucial test of our understanding of QCD at high-energy colliders.

Moreover, the production of a W and Z boson with one or two b jets represents a crucial irreducible background for several Higgs-boson production channels at the LHC. $Wb\bar{b}$ production is an irreducible background to WH associated production followed by the decay $H \to b\bar{b}$. This is a difficult channel but theoretically very interesting, since it can play a very important role in measuring the b-quark Yukawa coupling for a light Higgs boson at the LHC. Analogously, for a light Higgs boson, $Zb\bar{b}$ production is a background to ZH associated production followed by the decay $H \to b\bar{b}$. More importantly, for heavier Higgs bosons, if the b quarks in $Zb\bar{b}$ production decay leptonically, the $Zb\bar{b}$ production process can be a background to the inclusive production of a Higgs boson followed by the decay $H \to ZZ$ with each Z boson decaying leptonically. Finally, $Zb\bar{b}$ production is a background to searches for Higgs bosons with enhanced b-quark Yukawa couplings, produced in $Hb\bar{b}$ associated production followed by the decay $H \to \mu^+\mu^-$ or $H \to \tau^+\tau^-$ [5].

All Higgs-boson production channels have been calculated including at least next-to-leading order (NLO) QCD corrections (see, e. g., Ref. [6] for a recent review). The hadronic cross sections for $gg \to H$ and associated WH and ZH production are also known at next-to-next-to-leading order (NNLO) in QCD, Refs. [7, 8, 9, 10, 11, 12, 13, 14, 15, 16, 17] and Refs. [18, 19, 20], respectively. The NLO electroweak corrections to these processes have been calculated as well (see Ref. [21] and references therein ($gg \to H$) and Ref. [22] (WH, ZH)). The cross section for $Hb\bar{b}$ associated production is known at NLO in QCD including full b-quark mass effects [23, 24, 25, 26].

The production of a W or a Z boson with up to two jets, one of which is a b jet, has been calculated including NLO QCD corrections in the variable-flavor scheme (VFS) [27, 28, 29], while the production of a W or Z boson with two b jets has been derived at NLO in QCD using the fixed-flavor scheme (FFS), first in the massless b-quark approximation [30, 31, 32, 33, 34, 35] and more recently including full b-quark mass effects [36, 37, 38]. In the FFS only massless-quark densities are considered in the initial state, hence the alternative name of 4-flavor-number scheme (4FNS), while in a VFS an initial-state b-quark density is introduced, hence the alternative name of 5-flavor-number scheme (5FNS). The two schemes amount to a different ordering of the perturbative series for the production cross section: in the 4FNS the perturbative series is ordered strictly by powers of the strong coupling α_s, whereas in the 5FNS the introduction of a b-quark parton distribution function (PDF) allows to resum terms of the form $\alpha_s^n \ln(m_b^2/M^2)^m$ at all orders in α_s (for fixed order of logarithms m), where M represents the upper integration limit of the b-quark transverse momentum and can be thought to be of the order of M_W or M_Z. While the two approaches can give very different results at the leading or lowest order (LO) in QCD, starting at NLO in QCD they have been shown to be consistent within their respective theoretical uncertainties for both $H + 1\,b$-jet production [39, 40, 41] (for a brief review see also Ref. [26]) and single-top production [42]. Recently, $W + 1\,b$-jet production has been calculated by consistently combining both NLO 4FNS and 5FNS calculations [43]. Since the relevance of the logarithms resummed in the VFS approach varies with the kinematic regime considered, combining the two calculations improves the accuracy of the theoretical prediction for $W + 1\,b$-jet production. A similar study is currently in progress for $Z + 1\,b$-jet production [44]. Improving the predictions for $Z + 1\,b$-jet production will be particularly relevant at the LHC, where this process allows for a direct determination of the b-quark PDF, to be used in the prediction of $H + 1\,b$-jet

production, a discovery channel for beyond-the-SM Higgs bosons with enhanced b-quark Yukawa couplings.

In this paper we provide results for $Wb\bar{b}$ and $Zb\bar{b}$ production at the LHC, keeping the W and Z boson on shell and with both b jets tagged in the final state, i. e. we focus on the $W/Z + 2\,b$-jet case. We include NLO QCD corrections and full b-quark mass effects. The corresponding results for $Wb\bar{b}$ and $Zb\bar{b}$ production at the Tevatron have been presented in Refs. [36, 37, 38]. The details of the NLO QCD calculations used to compute the NLO cross sections in this paper can be found in Refs. [36, 37, 38]. In this paper we focus on presenting results for the total production cross sections and kinematic distributions that are of interest to LHC physics. Using the MCFM package [45], we compare our results to those obtained by neglecting the b-quark mass at NLO in QCD. A non-zero b-quark mass mainly affects phase space regions where the relevant kinematic observable, such as the transverse momentum of the bottom quarks or the invariant mass of the b-quark pair, are of the order of m_b. Indeed, this is the reason why b-quark mass effects cannot be neglected in studies of $W/Z + n$-jet production ($n = 1, 2$) with at least one b jet, as has been discussed for the $n = 2$ case in Refs. [28, 29] and for the $n = 1$ case in [43].

The paper is organized as follows: in Section II we briefly describe our choice of input parameters, cuts, jet-identification algorithm, and observables, while we present numerical results and a discussion of the b-quark mass effects for $Wb\bar{b}$ and $Zb\bar{b}$ production in Section III and Section IV, respectively. Section V contains our conclusions.

II. GENERAL SETUP

The results for both $Wb\bar{b}$ and $Zb\bar{b}$ production presented in this paper have been obtained for the LHC pp collider running at a center-of-mass energy of either $\sqrt{s} = 10$ TeV or $\sqrt{s} = 14$ TeV. While we only provide kinematic distributions obtained with a center-of-mass energy of $\sqrt{s} = 14$ TeV, we compare the total cross sections obtained for center-of-mass energies of $\sqrt{s} = 10$ TeV and $\sqrt{s} = 14$ TeV in Tables I and II. The mass of the bottom quark is taken to be $m_b = 4.62$ GeV. Results in the massless b-quark approximation have been obtained using the MCFM code (version 5.4) [45]. The top-quark mass, entering in the virtual corrections, is set to $m_t = 172.6$ GeV. In the case of $Wb\bar{b}$ production we use $M_W = 80.44$ GeV, while for $Zb\bar{b}$ production we use $M_Z = 91.1876$ GeV and derive M_W from the relation $M_W = M_Z \cos\theta_W$.

In both cases we assume $\sin^2\theta_W = 0.223$. We work in the electroweak G_μ input scheme and replace the fine structure constant $\alpha(0) = e^2/(4\pi)$ by $\alpha(G_\mu) = \frac{\sqrt{2}}{\pi} G_\mu M_W^2 \sin^2\theta_W$ with the Fermi constant $G_\mu = 1.16639 \cdot 10^{-5}\,\mathrm{GeV}^{-2}$. The W-boson coupling to quarks is proportional to the Cabibbo-Kobayashi-Maskawa (CKM) matrix elements. We use non-zero CKM matrix elements for the first two quark generations, $V_{ud} = V_{cs} = 0.974$ and $V_{us} = V_{cd} = 0.227$, while we neglect the contribution of the third generation, since it is suppressed either by the initial-state quark PDFs or by the corresponding CKM matrix elements.

The LO results are based on the one-loop evolution of α_s and the CTEQ6L1 set of PDFs [46], with $\alpha_s^{LO}(M_Z) = 0.130$, while the NLO results use the two-loop evolution of α_s and the CTEQ6M set of PDFs, with $\alpha_s^{NLO}(M_Z) = 0.118$. In the calculation of the parton luminosity we assume five light flavors in the initial state, but we have verified that including the b-quark PDF has a negligible effect ($< 0.1\%$) on the $W/Zb\bar{b}$ cross section. We implement the k_T jet algorithm [47, 48, 49, 50] with a pseudo-cone size of $R = 0.7$ and we recombine the parton momenta within a jet using the so called covariant E-scheme [48]. We checked that our implementation of the k_T jet algorithm coincides with the one in MCFM. We require all events to have a b-jet pair in the final state, with a transverse momentum larger than either 15 GeV or 25 GeV, in order to study the dependence on the b-jet transverse-momentum cut. We also require that the pseudorapidities of both b jets satisfy $|\eta^{b,\bar{b}}| < 2.5$. We impose the same p_T and $|\eta|$ cuts also on the extra jet that may arise due to hard non-collinear real emission of a parton, i. e. in the processes $W/Zb\bar{b} + g$ or $W/Zb\bar{b} + q(\bar{q})$. This hard non-collinear extra parton is treated either *inclusively* or *exclusively*. In the *inclusive* case we include both two- and three-jet events, while in the *exclusive* case we require exactly two jets in the event. Two-jet events consist of a b-jet pair that may also include a final-state light parton (gluon or quark) due to the applied recombination procedure. On the other hand, three-jet events consist of events containing a b-jet pair plus an extra light jet. We notice that, at NLO in QCD, all jets in three-jet events consist of a single parton.

For both $Wb\bar{b}$ and $Zb\bar{b}$ production we provide results for the total cross section (σ) and the following kinematic distributions: $d\sigma/dp_T^{b,l}$, $d\sigma/dp_T^{b,sl}$, $d\sigma/dp_T^{W/Z}$, $d\sigma/d\eta^{b,l}$, $d\sigma/d\eta^{b,sl}$, $d\sigma/d\eta^{W/Z}$, $d\sigma/dm_{b\bar{b}}$, and $d\sigma/dR^{b\bar{b}}$, where $p_T^{b,l}$, $p_T^{b,sl}$, and $p_T^{W/Z}$ are the transverse momenta of the leading b jet (i. e. leading in p_T), the subleading b jet and of the W or Z boson, $\eta^{b,l}$, $\eta^{b,sl}$, and $\eta^{W/Z}$ are the corresponding pseudorapidities, $m_{b\bar{b}}$ is the invariant mass of the $b\bar{b}$ pair, and $R_{b\bar{b}}$ is their relative separation in the pseudorapidity-azimuthal angle plane,

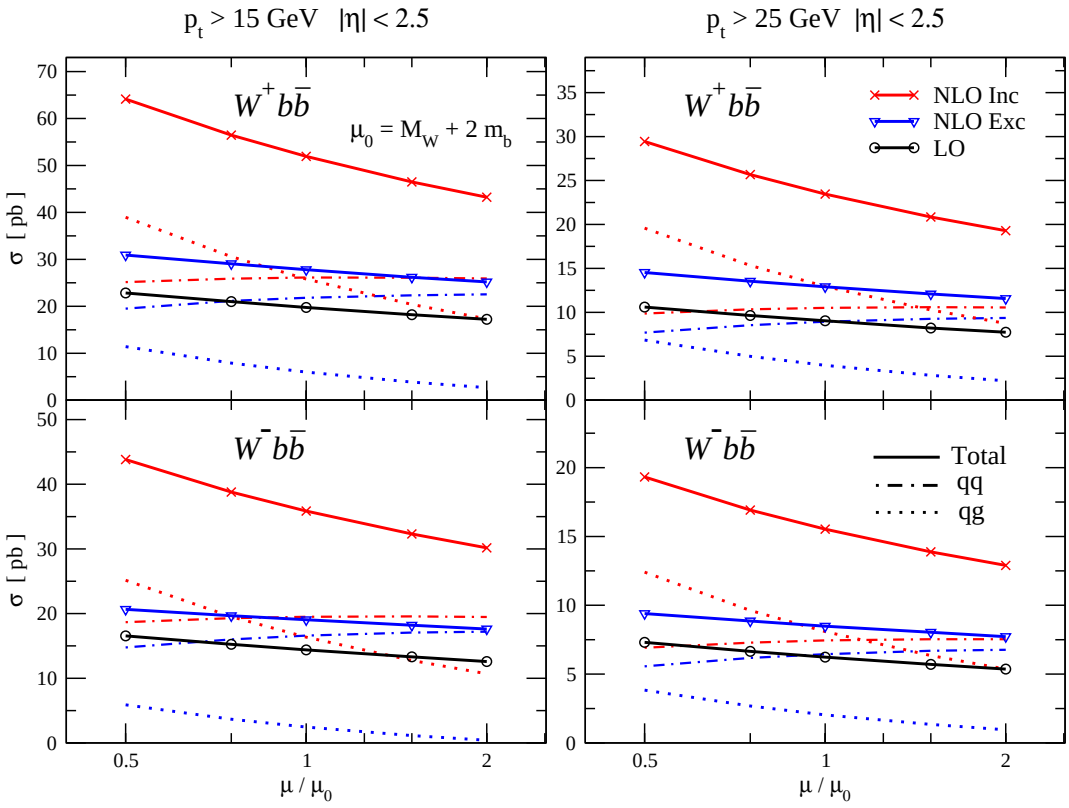

FIG. 1: Dependence of the LO (black, solid), NLO *exclusive* (blue, solid), and NLO *inclusive* (red, solid) total cross sections for $W^+b\bar{b}$ and $W^-b\bar{b}$ production on the renormalization/factorization scales, including full b-quark mass effects, when $\mu = \mu_r = \mu_f$ is varied between $\mu_0/2$ and $2\mu_0$ (with $\mu_0 = M_W + 2m_b$). We also show the individual channels, $q\bar{q}'$ (dash-dotted) and $qg + \bar{q}g$ (dotted), for the *inclusive* (red) and *exclusive* (blue) cases.

$$R_{b\bar{b}} = \sqrt{(\eta^{b,l} - \eta^{b,sl})^2 + (\phi^{b,l} - \phi^{b,sl})^2}.$$

III. $Wb\bar{b}$ PRODUCTION

At tree level, the production of a W boson with a pair of bottom quarks consists of just one process, $q\bar{q}' \to Wb\bar{b}$. In order to compute this process at NLO in QCD one needs to include one-loop virtual corrections to $q\bar{q}' \to Wb\bar{b}$ as well as all real radiation corrections with up to one extra parton in the final state, i. e. $q\bar{q}' \to Wb\bar{b}+g$ and $qg(\bar{q}g) \to Wb\bar{b}+q'(\bar{q}')$. Details of the calculation have been given in Refs. [36, 38] and will not be repeated here.

We note that, contrary to a $p\bar{p}$ collider like the Tevatron, at a pp collider like the LHC

TABLE I: LO, NLO *inclusive*, and NLO *exclusive* cross sections for $W^+b\bar{b}$ and $W^-b\bar{b}$ production at both $\sqrt{s} = 10$ TeV and $\sqrt{s} = 14$ TeV, for two different values of the b-jet transverse-momentum selection cut, and for a zero (obtained with MCFM) and non-zero b-quark mass. The central values correspond to $\mu_r = \mu_f = \mu_0 = M_W + 2m_b$, while the upper and lower bounds represent the maximal upper and lower variation obtained when varying $\mu_r = \mu_f$ between $\mu_0/2$ and $2\mu_0$.

	$W^+b\bar{b}$				$W^-b\bar{b}$			
	$p_T^b > 15$ GeV		$p_T^b > 25$ GeV		$p_T^b > 15$ GeV		$p_T^b > 25$ GeV	
	$m_b \neq 0$	$m_b = 0$	$m_b \neq 0$	$m_b = 0$	$m_b \neq 0$	$m_b = 0$	$m_b \neq 0$	$m_b = 0$
	$\sqrt{s} = 10$ TeV							
σ_{LO} (pb)	$14.4^{+2.6}_{-2.1}$	$15.5^{+2.7}_{-2.2}$	$6.49^{+1.3}_{-1.0}$	$6.67^{+1.3}_{-1.1}$	$9.77^{+1.7}_{-1.4}$	$10.5^{+1.8}_{-1.5}$	$4.15^{+0.83}_{-0.66}$	$4.27^{+0.83}_{-0.68}$
$\sigma_{NLO,inc}$ (pb)	$33.6^{+7.8}_{-5.6}$	$36.4^{+8.1}_{-6.2}$	$14.6^{+3.6}_{-2.5}$	$15.1^{+3.6}_{-2.7}$	$22.1^{+4.9}_{-3.5}$	$24.0^{+5.2}_{-3.9}$	$9.16^{+2.2}_{-1.5}$	$9.49^{+2.1}_{-1.7}$
$\sigma_{NLO,exc}$ (pb)	$18.6^{+1.7}_{-1.6}$	$20.3^{+1.7}_{-1.8}$	$8.37^{+0.84}_{-0.77}$	$8.67^{+0.85}_{-0.87}$	$12.3^{+0.86}_{-0.90}$	$13.4^{+0.9}_{-1.2}$	$5.29^{+0.48}_{-0.45}$	$5.50^{+0.43}_{-0.51}$
	$\sqrt{s} = 14$ TeV							
σ_{LO} (pb)	$19.8^{+3.1}_{-2.5}$	$21.3^{+3.2}_{-2.7}$	$9.02^{+1.6}_{-1.3}$	$9.26^{+1.6}_{-1.3}$	$14.4^{+2.1}_{-1.8}$	$15.5^{+2.2}_{-2.0}$	$6.24^{+1.1}_{-0.87}$	$6.42^{+1.1}_{-0.91}$
$\sigma_{NLO,inc}$ (pb)	$51.9^{+12}_{-8.7}$	$56.3^{+13}_{-9.6}$	$23.4^{+6.0}_{-4.2}$	$24.3^{+5.9}_{-4.5}$	$35.8^{+7.9}_{-5.7}$	$39.0^{+8.5}_{-6.4}$	$15.5^{+3.8}_{-2.6}$	$16.1^{+3.7}_{-2.8}$
$\sigma_{NLO,exc}$ (pb)	$27.8^{+3.1}_{-2.5}$	$30.4^{+3.5}_{-2.8}$	$12.9^{+1.6}_{-1.3}$	$13.4^{+1.6}_{-1.5}$	$19.0^{+1.6}_{-1.4}$	$20.8^{+1.7}_{-1.5}$	$8.49^{+0.90}_{-0.77}$	$8.83^{+0.93}_{-0.81}$

the cross sections for $W^+b\bar{b}$ and $W^-b\bar{b}$ are different, because the two processes depend on different quark/antiquark PDFs that are not symmetrically distributed between the two incoming nucleons. In the following we will provide results separately for both production processes.

In Fig. 1 we illustrate the renormalization- and factorization-scale dependence of the LO and NLO total cross sections obtained for a massive b quark, when $\mu = \mu_r = \mu_f$ is varied between $\mu_0/2$ and $2\mu_0$, with $\mu_0 = M_W + 2m_b$. We immediately notice that the impact of NLO QCD corrections is very large, in particular in the *inclusive* case, where they increase the LO cross section by a factor between two and three depending on the scale. We also notice that the scale dependence of the NLO cross section is worse than (*inclusive* case) or comparable to (*exclusive* case) the scale dependence of the LO cross section. This is different from what has been observed for the Tevatron [36, 38], and was first pointed out in a calculation with massless bottom quarks [35]. It is just a reminder of the fact

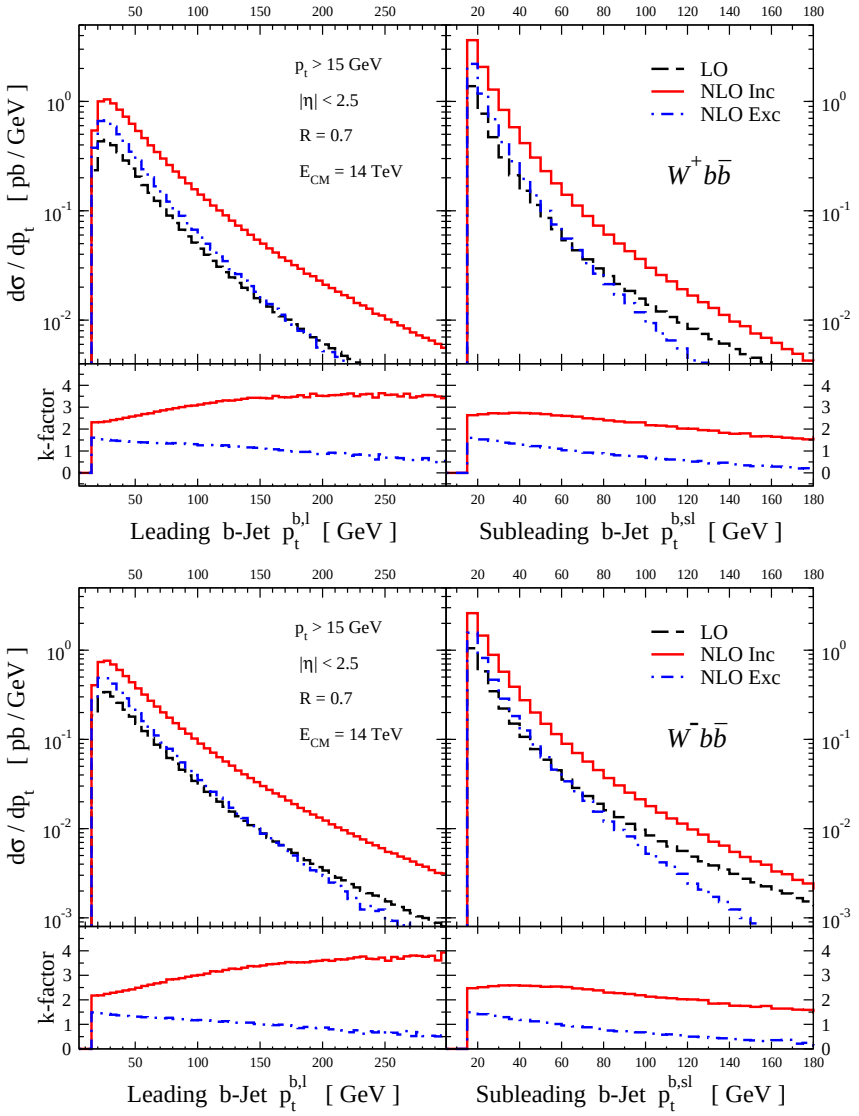

FIG. 2: LO (black, dashed), NLO *inclusive* (red, solid) and NLO *exclusive* (blue, dot-dashed) transverse momentum distributions for the b jet with the leading (left hand side) and subleading (right hand side) transverse momentum in $W^+b\bar{b}$ (upper plots) and $W^-b\bar{b}$ (lower plots) production. The lower window shows a bin-by-bin K factor, for the *inclusive* (red, solid) and *exclusive* (blue, dot-dashed) cases.

that, at a given perturbative order, the uncertainty due to the residual renormalization- and factorization-scale dependence may underestimate the theoretical uncertainty due to missing higher-order corrections. A realistic determination of this uncertainty is usually much more complex and requires a thorough understanding of the perturbative structure of the cross section, in particular at the lowest orders of the perturbative expansion. In $Wb\bar{b}$ production

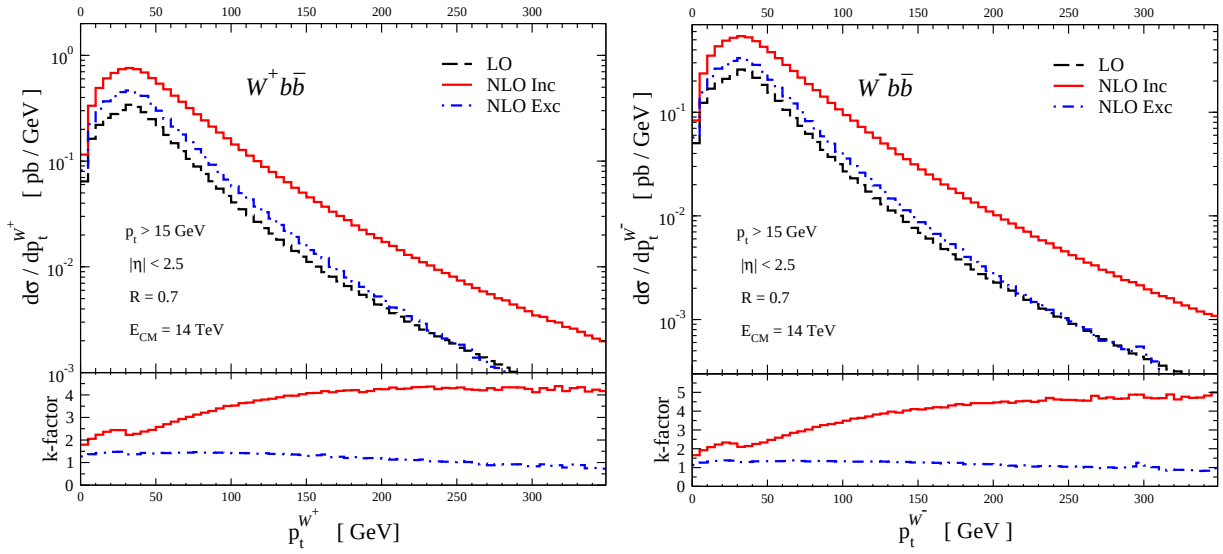

FIG. 3: LO (black, dashed), NLO *inclusive* (red, solid) and NLO *exclusive* (blue, dot-dashed) transverse momentum distributions for the W^+ (left hand side) and W^- (right hand side) bosons in $W^+b\bar{b}$ and $W^-b\bar{b}$ production respectively. The lower window shows a bin-by-bin K factor, for the *inclusive* (red, solid) and *exclusive* (blue, dot-dashed) cases.

the NLO QCD corrections introduce a new, numerically important production channel not present at LO, as will be discussed in more detail below. Therefore, only at NLO the scale dependence of the cross sections starts to be a meaningful measure of the behavior of the perturbative expansion.

In order to understand better the behavior of the $W^+b\bar{b}$ and $W^-b\bar{b}$ cross section, we also show in Fig. 1 the scale dependence of the individual parton-level channels. We notice that although the $qg(\bar{q}g) \to W^{\pm}b\bar{b} + q'(\bar{q}')$ channel appears for the first time at NLO in the perturbative expansion of the $Wb\bar{b}$ cross section, it is actually a tree level contribution and, as such, introduces a large scale dependence in the calculation that will be moderated only by adding (still unknown) NNLO corrections. The reason why this becomes so evident at the LHC, while it is not at the Tevatron, is because the $qg(\bar{q}g) \to W^{\pm}b\bar{b} + q'(\bar{q}')$ channel is enhanced by the correspondingly large initial-state gluon PDF. The NLO $Wb\bar{b}$ total cross section is particularly affected by this process because there is no gluon-initiated process at LO. Finally, the impact of the $qg(\bar{q}g) \to W^{\pm}b\bar{b}+q'(\bar{q}')$ channel on the scale dependence of the total cross section is larger in the *inclusive* than in the *exclusive* case because the *exclusive* cross section by definition discriminates against processes with more than two jets in the

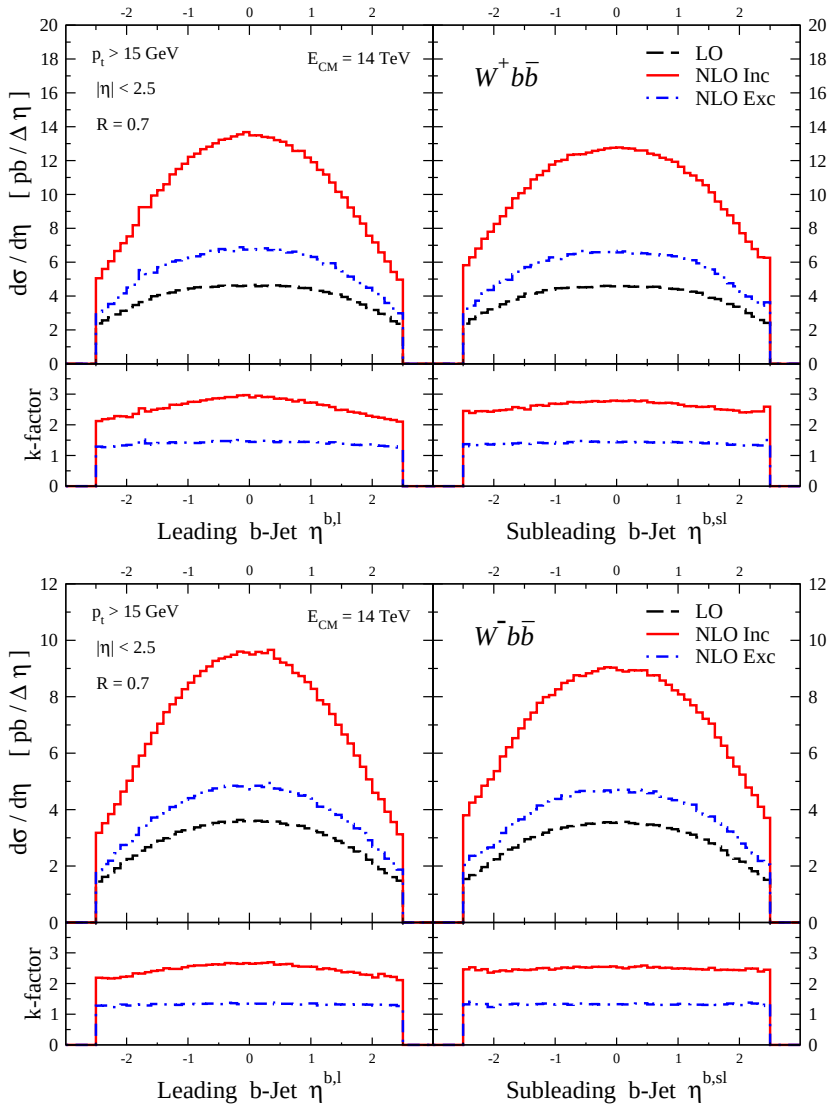

FIG. 4: LO (black, dashed), NLO *inclusive* (red, solid) and NLO *exclusive* (blue, dot-dashed) pseudorapidity distributions for the b jet with the leading (left hand side) and subleading (right hand side) transverse momentum in $W^+b\bar{b}$ (upper plots) and $W^-b\bar{b}$ (lower plots) production. The lower window shows a bin-by-bin K factor, for the *inclusive* (red, solid) and *exclusive* (blue, dot-dashed) cases.

final state. Figure 1 also shows the effect of lowering the cut on the transverse momentum of the b jets. Lowering the cut from $p_T^b > 25$ GeV to $p_T^b > 15$ GeV almost doubles the cross section and can therefore be a crucial factor in deciding which selection cuts to use for b jets.

In Table I we present both LO and NLO total cross sections separately for $W^+b\bar{b}$

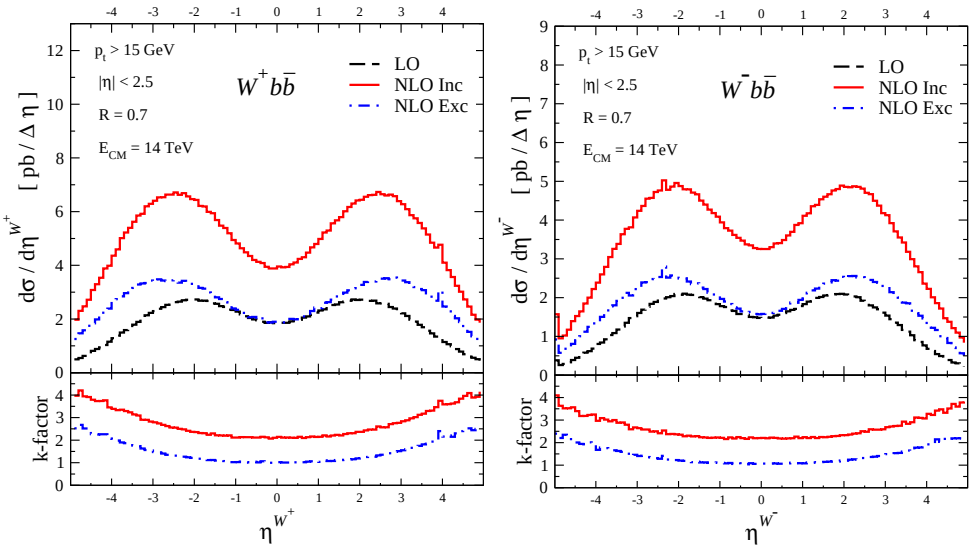

FIG. 5: LO (black, dashed), NLO *inclusive* (red, solid) and NLO *exclusive* (blue, dot-dashed) pseudorapidity distributions for the W^+ (left hand side) and W^- (right hand side) bosons in $W^+b\bar{b}$ and $W^-b\bar{b}$ production respectively. The lower window shows a bin-by-bin K factor, for the *inclusive* (red, solid) and *exclusive* (blue, dot-dashed) cases.

and $W^-b\bar{b}$ production, including our estimate of the scale uncertainty due to the residual renormalization- and factorization-scale dependence. We provide results for both $p_T^b > 15$ GeV and $p_T^b > 25$ GeV, and for both center-of-mass energies, $\sqrt{s} = 14$ TeV and $\sqrt{s} = 10$ TeV. We also include the corresponding set of results obtained with MCFM for $m_b = 0$. Comparing the results from the massless approximation and our results with full b-quark mass dependence, one observes that for $p_T^b > 15$ GeV the massless approximation overestimates the total cross section by about 10%, while for $p_T^b > 25$ GeV the difference is a milder 3% (both for $\sqrt{s} = 10$ TeV and $\sqrt{s} = 14$ TeV). As expected, the more inclusive the treatment of the b jets the more important the b-quark mass effects become. This, for example, explains why for a complete NLO treatment of $W + 1\,b$-jet production, the contributions from the $Wb\bar{b}$ production process must be calculated using the full b-quark mass dependence, as discussed in [43].

In Figs. (2)-(5) we show the transverse momentum (p_T) and pseudorapidity (η) distributions for the b jet with the leading and subleading transverse momentum and for the W boson for both $W^+b\bar{b}$ and $W^-b\bar{b}$ production. The results for these distributions, as well as for all other distributions presented in this paper, have been obtained with $\sqrt{s} = 14$ TeV

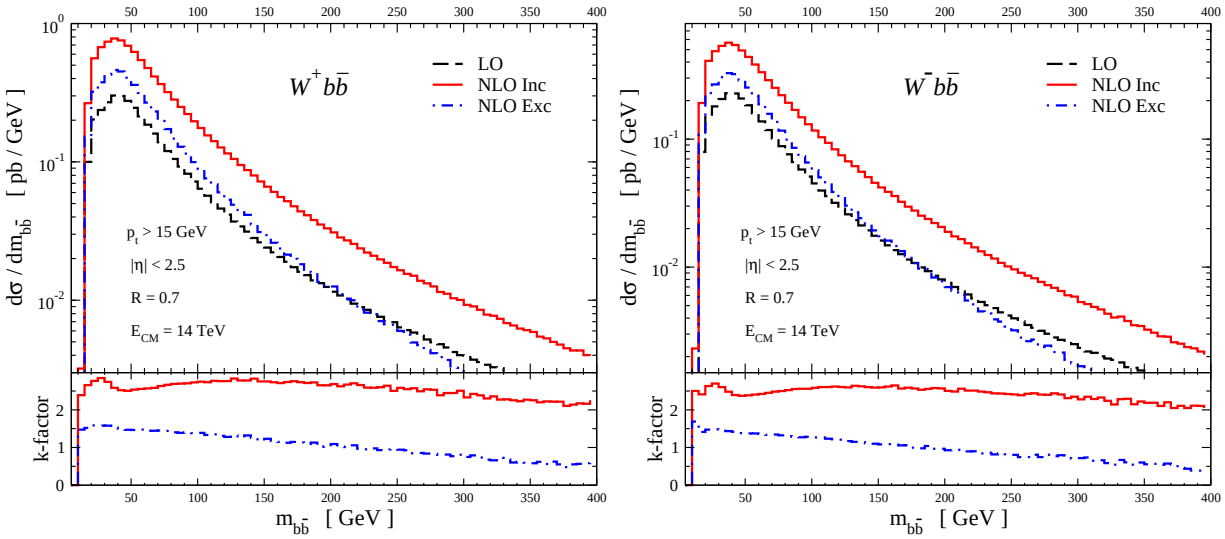

FIG. 6: LO (black, dashed), NLO *inclusive* (red, solid) and NLO *exclusive* (blue, dot-dashed) $b\bar{b}$-pair invariant mass distributions in $W^+b\bar{b}$ (left hand side) and $W^-b\bar{b}$ (right hand side) production. The lower window shows a bin-by-bin K factor, for the *inclusive* (red, solid) and *exclusive* (blue, dot-dashed) cases.

and by assuming $p_T^b > 15$ GeV and $|\eta^b| < 2.5$. The upper panels of each figure show the LO, NLO *inclusive* and NLO *exclusive* distributions, while the lower panels show the ratios $d\sigma^{inc}_{NLO}/d\sigma_{LO}$ and $d\sigma^{exc}_{NLO}/d\sigma_{LO}$, thereby providing a bin-by-bin K factor. In each figure we show the results obtained with the central scale choice $\mu_r = \mu_f = \mu_0 = M_W + 2m_b$. The distributions for the invariant mass of the two b jets ($m_{b\bar{b}}$) and for their relative separation in the pseudorapidity-azimuthal angle plane ($R_{b\bar{b}}$) are shown in Fig. (6) and (7), respectively.

Clearly, the NLO QCD corrections largely affect the kinematic distributions, resulting in considerable changes in their shapes, both in the *inclusive* and *exclusive* case. Figure (2) shows that at NLO in QCD the production of b jets at large p_T^b is consistently suppressed in the *exclusive* case, while in the *inclusive* case the cross section for the production of a leading b jet is enhanced, yielding K factors of about 2 in the low p_T^b region and of about 3.5 at large p_T^b. Similar features can be observed in the p_T^W distributions of Fig. (3). We note that this may have an impact especially on assessing the effects of experimental triggers on the lepton coming from the W-boson decay. The pseudorapidity distributions of the leading and sub-leading b jet of Figs. (4) and (5) in the *exclusive* case are enhanced by the NLO QCD corrections but their shape is barely affected, while in the *inclusive* case the increase

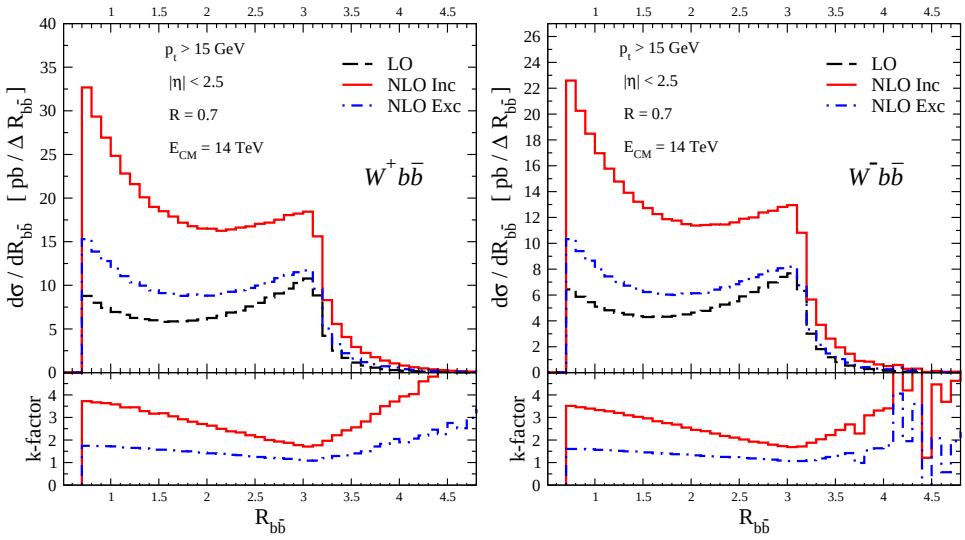

FIG. 7: LO (black, dashed), NLO *inclusive* (red, solid) and NLO *exclusive* (blue, dot-dashed) $R_{b\bar{b}}$ distributions in $W^+b\bar{b}$ (left hand side) and $W^-b\bar{b}$ (right hand side) production. The lower window shows a bin-by-bin K factor, for the *inclusive* (red, solid) and *exclusive* (blue, dot-dashed) cases.

of the η^b distribution of the leading b jet is more pronounced in the central region. The increase of the pseudorapidity distributions of the W bosons at NLO QCD, on the other hand, is more pronounced in the forward regions in both the *inclusive* and *exclusive* cases. Finally, we point out that the large positive corrections to the $R_{b\bar{b}}$ distributions of Fig. (7) in regions with low and large values of $R_{b\bar{b}}$ are especially pronounced in the *inclusive* case. Although these changes in shape are commonly seen in NLO QCD computations involving two or more jets, the large effects observed here in the *inclusive* case are a specific feature of $Wb\bar{b}$ production, originating from the tree-like qg-initiated contribution to the NLO QCD corrections, as one can easily deduce from comparing with the *exclusive* K factors.

Finally, we compared the distributions presented here to the ones produced by MCFM in the massless b-quark approximation. We agree very well, with only small (of the order of the change in the total cross sections shown in Table I) but noticeable deviations in regions where relevant kinematic observables become small, i. e. comparable to m_b. As an example, we show in Fig. 8 the comparison of the LO and NLO $m_{b\bar{b}}$ and $R_{b\bar{b}}$ distributions for $W^-b\bar{b}$ production obtained from the massive and massless b-quark calculations. Most of the difference between the massless and massive b-quark cross sections comes from the region of low invariant mass $m_{b\bar{b}}$, and are more pronounced for small values of $R_{b\bar{b}}$, both at LO and

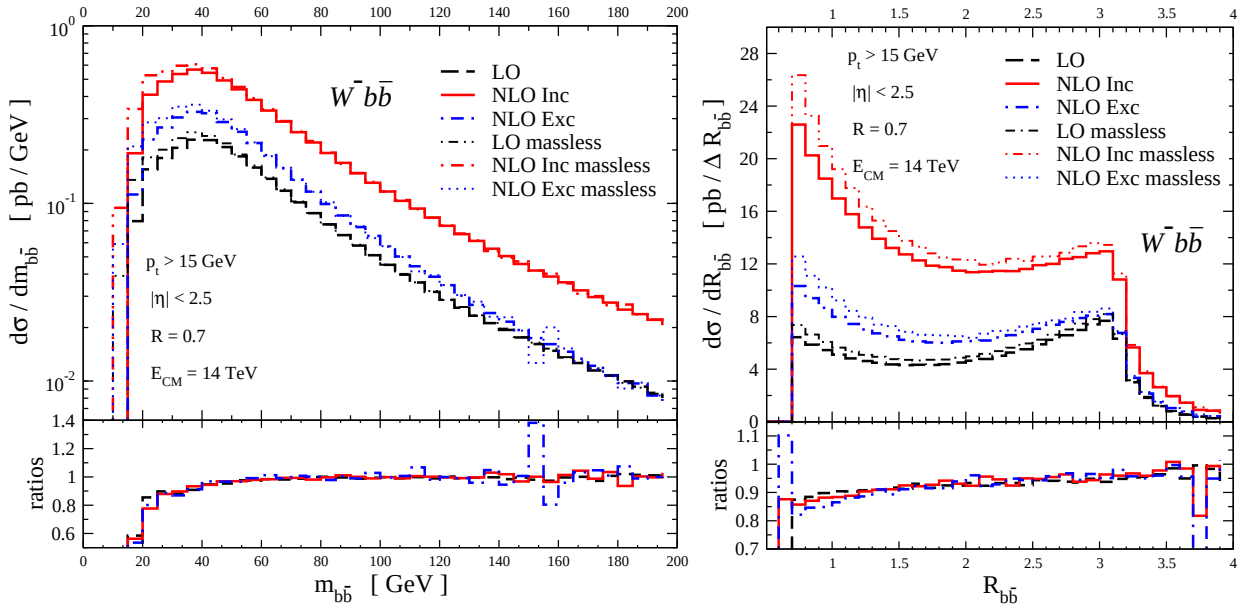

FIG. 8: LO (black), NLO *inclusive* (red) and NLO *exclusive* (blue) $m_{b\bar{b}}$ (left hand side) and $R_{b\bar{b}}$ (right hand side) distributions for $W^-b\bar{b}$ production derived from our calculation with $m_b \neq 0$ (LO: dashed, NLO *inclusive*: solid, NLO *exclusive*: dash-dotted) and from MCFM with $m_b = 0$ (LO: double-dashed/dotted, NLO *inclusive*: dashed/double-dotted, NLO *exclusive*: dotted). The lower window shows the ratio of the distributions for massive and massless b quarks, $d\sigma(m_b \neq 0)/d\sigma(m_b = 0)$ (LO: dashed, NLO *inclusive*: solid, NLO *exclusive*: dash-dotted).

at NLO, where the cross sections for $m_b \neq 0$ are consistently smaller than the ones with $m_b = 0$. This may indicate that a resummation of large logarithmic corrections may be in order when the two b jets become collinear. As can be seen by comparing the ratios of the LO and NLO cross sections in Fig. 8, the impact of a non-zero b-quark mass is almost not affected by including NLO QCD corrections and can be taken into account by rescaling the NLO result for massless bottom quarks with the ratio of the LO cross sections as discussed in [36].

IV. $Zb\bar{b}$ PRODUCTION

At tree level, the production of a Z boson with a pair of bottom quarks consists of two channels, namely $q\bar{q} \to Zb\bar{b}$ and $gg \to Zb\bar{b}$. At NLO in QCD one needs to include the one-loop virtual corrections to both tree-level processes as well as the real radiation corrections

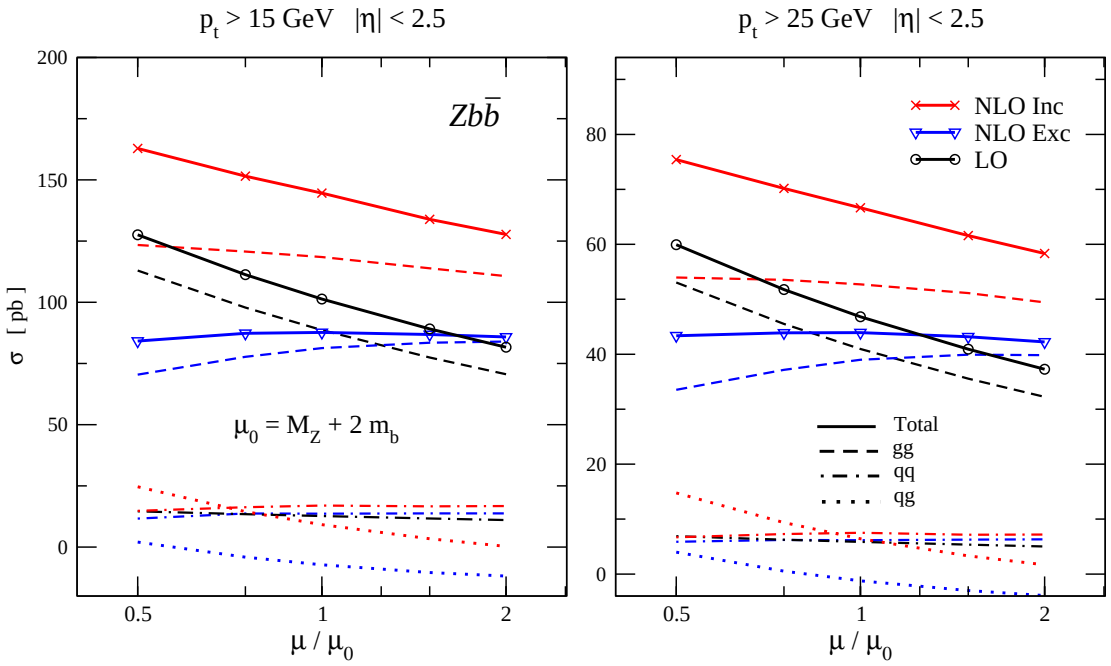

FIG. 9: Dependence of the LO (black, solid), NLO *exclusive* (blue, solid), and NLO *inclusive* (red, solid) total cross sections for $Zb\bar{b}$ production on the renormalization/factorization scales, including full b-quark mass effects, when $\mu = \mu_r = \mu_f$ is varied between $\mu_0/2$ and $2\mu_0$ (with $\mu_0 = M_Z + 2m_b$). We also show the individual channels, $q\bar{q}'$ (dash-dotted), $qg + \bar{q}g$ (dotted) and gg (dashed), for the *inclusive* (red) and *exclusive* (blue) cases.

with up to one extra parton in the final state, i.e. $q\bar{q} \to Zb\bar{b} + g$, $gg \to Zb\bar{b} + g$, and $qg(\bar{q}g) \to Zb\bar{b} + q(\bar{q})$. Details of the calculation have been given in Refs. [37, 38] and will not be repeated here.

As done in the case of $W^+b\bar{b}$ and $W^-b\bar{b}$ production in Section III, we start our discussion of $Zb\bar{b}$ cross sections at NLO QCD at the LHC by studying the renormalization- and factorization-scale dependence of the LO and NLO total cross sections. In Fig. 9 we show the scale dependence of the individual parton-level channels, as well as their sum, at LO and NLO in QCD for both the *inclusive* and *exclusive* case. As for $Wb\bar{b}$ production, we notice the pronounced scale dependence of the NLO total cross section to $qg(\bar{q}g) \to Zb\bar{b} + q(\bar{q})$. However, since in $Zb\bar{b}$ production both the LO and NLO cross sections also consist of a gg-initiated subprocess, the $qg(\bar{q}g) \to Zb\bar{b} + q(\bar{q})$ channel is not dominant at NLO and its effect is therefore less pronounced. Indeed, the scale dependence of the *exclusive* cross sec-

TABLE II: LO, NLO *inclusive*, and NLO *exclusive* cross sections for $Zb\bar{b}$ at both $\sqrt{s} = 10$ TeV and $\sqrt{s} = 14$ TeV, for two different values of the b-jet transverse-momentum selection cut, and for zero and non-zero b-quark mass. The central values correspond to $\mu_r = \mu_f = \mu_0 = M_Z + 2m_b$, while the upper and lower bounds represent the maximal upper and lower variations obtained when varying $\mu_r = \mu_f$ between $\mu_0/2$ and $2\mu_0$.

	$p_T^b > 15$ GeV		$p_T^b > 25$ GeV	
	$m_b \neq 0$	$m_b = 0$	$m_b \neq 0$	$m_b = 0$
	$\sqrt{s} = 10$ TeV			
σ_{LO} (pb)	55.1^{+16}_{-12}	57.6^{+18}_{-13}	$24.6^{+7.6}_{-5.4}$	$25.1^{+8.4}_{-5.9}$
$\sigma_{NLO,inc}$ (pb)	82.5^{+12}_{-11}	84.5^{+14}_{-12}	$36.0^{+3.9}_{-4.6}$	$36.1^{+6.4}_{-5.2}$
$\sigma_{NLO,exc}$ (pb)	$52.1^{+0.0}_{-1.7}$	$53.5^{+0.2}_{-2.4}$	$24.6^{+0.3}_{-1.2}$	$24.7^{+0.3}_{-1.6}$
	$\sqrt{s} = 14$ TeV			
σ_{LO} (pb)	101^{+26}_{-20}	106^{+30}_{-22}	$46.8^{+13.1}_{-9.6}$	$46.8^{+12.7}_{-9.9}$
$\sigma_{NLO,inc}$ (pb)	145^{+20}_{-17}	148^{+24}_{-19}	$66.6^{+8.8}_{-8.3}$	$66.1^{+10.5}_{-9.1}$
$\sigma_{NLO,exc}$ (pb)	$88.4^{+0.0}_{-3.0}$	$90.0^{+0.0}_{-1.6}$	$43.7^{+0.0}_{-1.6}$	$43.5^{+0.4}_{-1.9}$

tion actually greatly improves at NLO in QCD, while the scale dependence of the *inclusive* one is only mildly better than at LO, but not worse as it is the case in $Wb\bar{b}$ production.

In Table II we provide both LO and NLO total cross sections for $Zb\bar{b}$ production, including our estimate of the residual uncertainty due to only the renormalization- and factorization-scale dependence. We give results for two choices of p_T^b cuts, $p_T^b > 15$ GeV and $p_T^b > 25$ GeV, and for both center-of-mass energies, $\sqrt{s} = 14$ TeV and $\sqrt{s} = 10$ TeV. We compare the case of a massless and massive bottom quark and we observe that the effects of a non-zero b-quark mass are mild for $Zb\bar{b}$ production. Indeed, for $p_t^b > 15$ GeV the massless approximation mildly overestimates the total cross section by about $2 - 3\%$, which in the *inclusive* case is considerably smaller than the scale uncertainty. For $p_t^b > 25$ GeV the difference is basically gone. We remind, however, that this is not the case in more inclusive studies, like $Z + 1\,b$-jet production [44], where, as seen in $W + 1\,b$-jet production [43], one needs to consistently include full b-quark mass effects.

In Figs. (10)-(13) we show the transverse momentum (p_T) and pseudorapidity (η) distri-

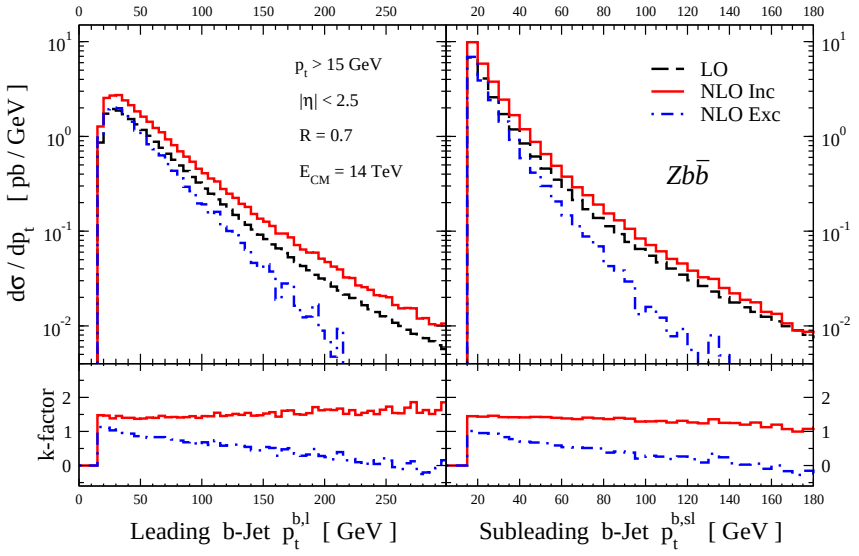

FIG. 10: LO (black, dashed), NLO *inclusive* (red, solid) and NLO *exclusive* (blue, dot-dashed) transverse momentum distributions for the b jet with the leading (left hand side) and subleading (right hand side) transverse momentum in $Zb\bar{b}$ production. The lower window shows the bin-by-bin K factor, for the *inclusive* (red, solid) and *exclusive* (blue, dot-dashed) cases.

butions for the b jet with the leading and subleading transverse momentum, and for the Z boson. As in the $Wb\bar{b}$ case, the upper parts of each figure show the LO, NLO *inclusive* and NLO *exclusive* distributions, while in the lower parts we provide the bin-by-bin K factors. We show results obtained by using the central scale choice $\mu_r = \mu_f = \mu_0 = M_Z + 2m_b$. As expected from the study of the scale dependence shown in Fig. (9), in the *exclusive* case the NLO QCD corrections reduce the cross sections as compared to the LO result, while in the *inclusive* case the NLO QCD corrections increase them. Figures (10) and (11) also show, in particular in the bin-by-bin K factors, that the NLO QCD corrections affect the shape of the *exclusive* transverse momentum distributions, with large negative corrections at large p_T where the bin-by-bin K factors become smaller than one, while the changes in the shape are much less pronounced in the *inclusive* case. Figures (12) and (13) show that NLO QCD corrections have hardly any effects on the shape of the pseudorapidity distributions. The distributions for the invariant mass of the two b jets ($m_{b\bar{b}}$) and for their relative distance ($R_{b\bar{b}}$) are shown in Figs. (14) and (15) respectively. We notice that, although in a much milder fashion than for $Wb\bar{b}$ production, in the *inclusive* case NLO QCD corrections enhance the regions at small and large values of $R_{b\bar{b}}$.

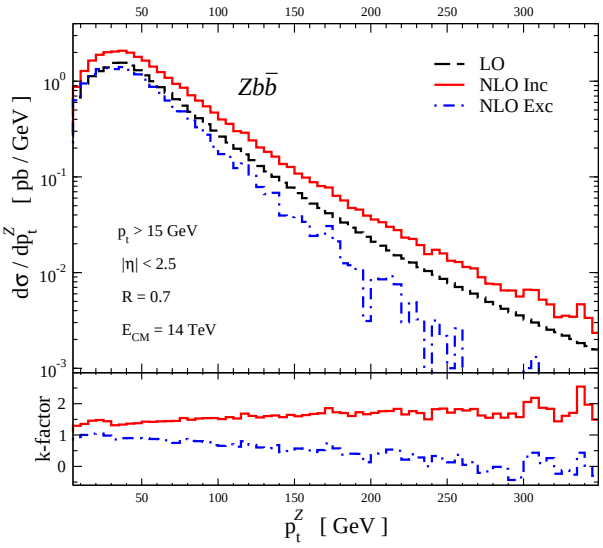

FIG. 11: LO (black, dashed), NLO *inclusive* (red, solid) and NLO *exclusive* (blue, dot-dashed) transverse momentum distributions for the Z boson in $Zb\bar{b}$. The lower window shows the bin-by-bin K factor, for the *inclusive* (red, solid) and *exclusive* (blue, dot-dashed) cases.

Finally, in Fig. 16 we compare the LO and NLO $m_{b\bar{b}}$ and $R_{b\bar{b}}$ distributions for $Zb\bar{b}$ production obtained from the massive and massless b-quark calculations. The results with $m_b = 0$ have been obtained using MCFM. Most of the difference is seen in the region of low invariant mass $m_{b\bar{b}}$, and are more noticeable for small values of $R_{b\bar{b}}$. In all regions though the impact of a non-zero b-quark mass is almost not affected by including NLO QCD corrections, and can be taken into account by rescaling the NLO result for massless bottom quarks with the ratio of the LO cross sections as discussed in [37].

V. CONCLUSIONS

A reliable theoretical prediction for W and Z production with b jets will be crucial for many Higgs-boson searches and studies at the LHC. In this paper we have presented a study of W and Z boson production with two b jets at the LHC including full b-quark mass effects, based on the NLO QCD calculation of $Wb\bar{b}$ and $Zb\bar{b}$ production presented in Refs. [36, 37, 38]. We have presented numerical results for the total $Wb\bar{b}$ and $Zb\bar{b}$ production cross sections, as well as for a number of kinematic distributions interesting to LHC physics, for both massive (our calculation) and massless bottom quarks (as implemented in MCFM).

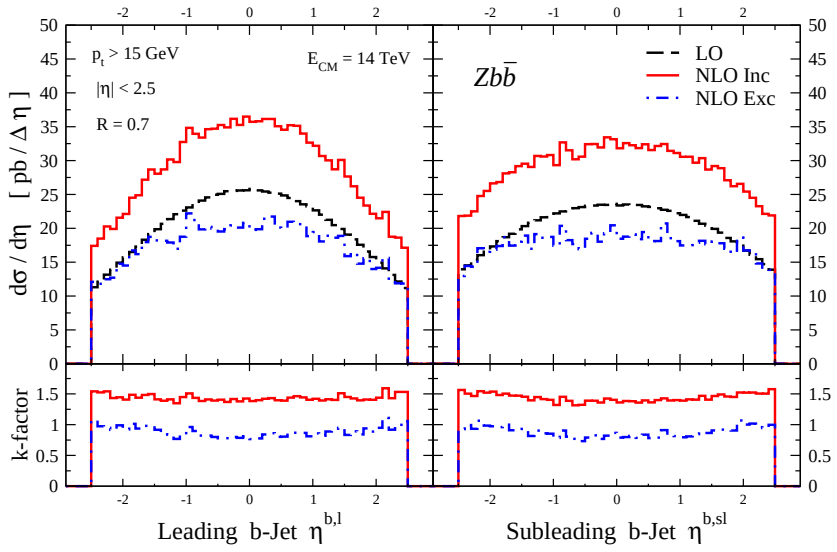

FIG. 12: LO (black, dashed), NLO *inclusive* (red, solid) and NLO *exclusive* (blue, dot-dashed) pseudorapidity distributions for the b jet with the leading (left hand side) and subleading (right hand side) transverse momentum in $Zb\bar{b}$ production. The lower window shows the bin-by-bin K factor, for the *inclusive* (red, solid) and *exclusive* (blue, dot-dashed) cases.

The $Wb\bar{b}$ cross sections at NLO QCD still suffer from a large theoretical uncertainty due to the unphysical renormalization- and factorization-scale dependence, which is particularly pronounced in the *inclusive* case, and further theoretical improvements are warranted. In the case of $Zb\bar{b}$ production, the NLO QCD cross sections are well behaved, i. e. exhibit only a mild residual scale dependence, in particular in the *exclusive* case. The shape of distributions is changed significantly by NLO QCD corrections, such that they can not be correctly described by global K-factor rescalings. This is more dramatic in the case for $Wb\bar{b}$ production, in view of which including resummation effects, as well as consistent NLO showering, might be of considerable importance.

The b-quark mass effects can impact the shape of the kinematic distributions, as shown on the example of the $m_{b\bar{b}}$ and $R_{b\bar{b}}$ distributions, in particular in phase space regions where the relevant kinematic observable is of the order of m_b. Apart from these regions, however, these effects can be approximated by rescaling the NLO cross section for $m_b = 0$ with the ratio of LO cross sections for massive and massless bottom quarks as discussed in detail in [36, 37]. The total production cross sections are reduced by b-quark mass effects, and the effect is more pronounced the smaller the applied p_T^b cut. However, these effects are in

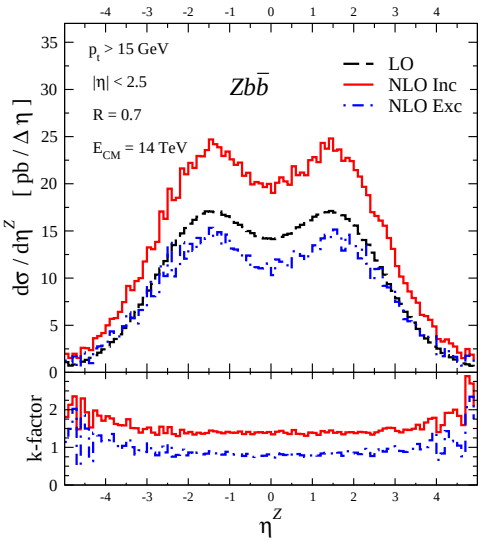

FIG. 13: LO (black, dashed), NLO *inclusive* (red, solid) and NLO *exclusive* (blue, dot-dashed) pseudorapidity distributions for the Z boson in $Zb\bar{b}$ production. The lower window shows the bin-by-bin K factor, for the *inclusive* (red, solid) and *exclusive* (blue, dot-dashed) cases.

most cases smaller than the residual scale dependence at NLO in QCD, especially in $Wb\bar{b}$ production for the *inclusive* case.

Acknowledgements

F. F. C. and L. R. would like to thank the Theory Division of CERN for its kind hospitality and support during the *From LHC to Future Colliders* CERN Theory Institute, where part of the work presented in this paper was completed. We thank in particular Chiara Mariotti, Sacha Nikitenko and the CMS Higgs working group for their interest and for very useful discussions. F. F. C. thanks Harald Ita for helpful discussions. The work of F. F. C. and L. R. is supported in part by the U.S. Department of Energy under grants DE-FG03-91ER40662 and DE-FG02-97IR41022 respectively. The work of D. W. is supported in part by the National Science Foundation under grants NSF-PHY-0757691 and NSF-PHY-0547564.

[1] T. Aaltonen et al. (CDF) (2008), arXiv:0812.4458 [hep-ex].

[2] C. Neu, E. Thomson, and J. Heinrich (CDF) (2008), CDF note 9321.

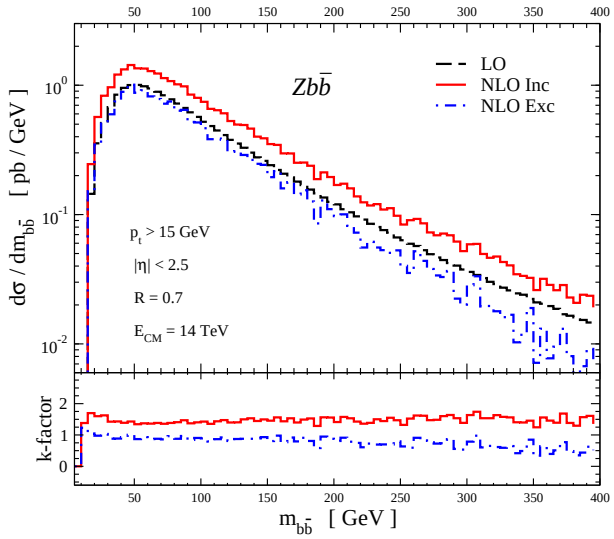

FIG. 14: LO (black, dashed), NLO *inclusive* (red, solid) and NLO *exclusive* (blue, dot-dashed) $b\bar{b}$-pair invariant-mass distributions for $Zb\bar{b}$ production. The lower window shows the bin-by-bin K factor, for the *inclusive* (red, solid) and *exclusive* (blue, dot-dashed) cases.

[3] V. M. Abazov et al. (D0), Phys. Rev. Lett. **94**, 091802 (2005), hep-ex/0410062.

[4] V. M. Abazov et al. (D0), Phys. Rev. Lett. **94**, 161801 (2005), hep-ex/0410078.

[5] C. Kao, D. A. Dicus, R. Malhotra, and Y. Wang (2007), arXiv:0711.0232 [hep-ph].

[6] N. E. Adam et al. (2008), arXiV:0803.1154 [hep-ph].

[7] R. V. Harlander, Phys. Lett. **B492**, 74 (2000), hep-ph/0007289.

[8] R. V. Harlander and W. B. Kilgore, Phys. Rev. **D64**, 013015 (2001), hep-ph/0102241.

[9] R. V. Harlander and W. B. Kilgore, Phys. Rev. Lett. **88**, 201801 (2002), hep-ph/0201206.

[10] C. Anastasiou and K. Melnikov, Nucl. Phys. **B646**, 220 (2002), hep-ph/0207004.

[11] C. Anastasiou, K. Melnikov, and F. Petriello, Phys. Rev. Lett. **93**, 262002 (2004), hep-ph/0409088.

[12] V. Ravindran, J. Smith, and W. L. van Neerven, Nucl. Phys. **B665**, 325 (2003), hep-ph/0302135.

[13] S. Catani, D. de Florian, and M. Grazzini, JHEP **05**, 025 (2001), hep-ph/0102227.

[14] S. Catani, D. de Florian, M. Grazzini, and P. Nason, JHEP **07**, 028 (2003), hep-ph/0306211.

[15] G. Bozzi, S. Catani, D. de Florian, and M. Grazzini, Nucl. Phys. **B737**, 73 (2006), hep-ph/0508068.

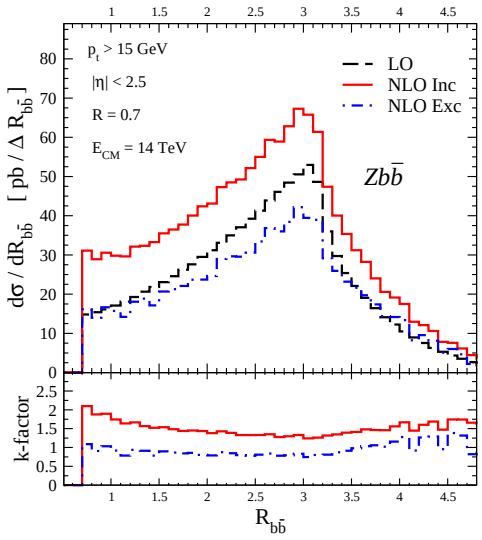

FIG. 15: LO (black, dashed), NLO *inclusive* (red, solid) and NLO *exclusive* (blue, dot-dashed) b-jet relative-distance distributions for $Zb\bar{b}$ production. The lower window shows the bin-by-bin K factor, for the *inclusive* (red, solid) and *exclusive* (blue, dot-dashed) cases.

[16] C. Anastasiou, R. Boughezal, and F. Petriello, JHEP **04**, 003 (2009), arXiv:0811.3458 [hep-ph].

[17] D. de Florian and M. Grazzini, Phys. Lett. **B674**, 291 (2009), arXiv:0901.2427 [hep-ph].

[18] T. Han and S. Willenbrock, Phys. Lett. **B273**, 167 (1991).

[19] S. Mrenna and C. P. Yuan, Phys. Lett. **B416**, 200 (1998), hep-ph/9703224.

[20] O. Brein, A. Djouadi, and R. Harlander, Phys. Lett. **B579**, 149 (2004), hep-ph/0307206.

[21] S. Actis, G. Passarino, C. Sturm, and S. Uccirati, Phys. Lett. **B670**, 12 (2008), arXiv:0809.1301 [hep-ph].

[22] M. L. Ciccolini, S. Dittmaier, and M. Krämer, Phys. Rev. **D68**, 073003 (2003), hep-ph/0306234.

[23] S. Dawson, C. B. Jackson, L. Reina, and D. Wackeroth, Phys. Rev. **D69**, 074027 (2004), hep-ph/0311067.

[24] S. Dittmaier, M. Krämer, and M. Spira, Phys. Rev. **D70**, 074010 (2004), hep-ph/0309204.

[25] S. Dawson, C. B. Jackson, L. Reina, and D. Wackeroth, Phys. Rev. Lett. **94**, 031802 (2005), hep-ph/0408077.

[26] S. Dawson, C. B. Jackson, L. Reina, and D. Wackeroth, Int. J. Mod. Phys. **A20**, 3353 (2005),

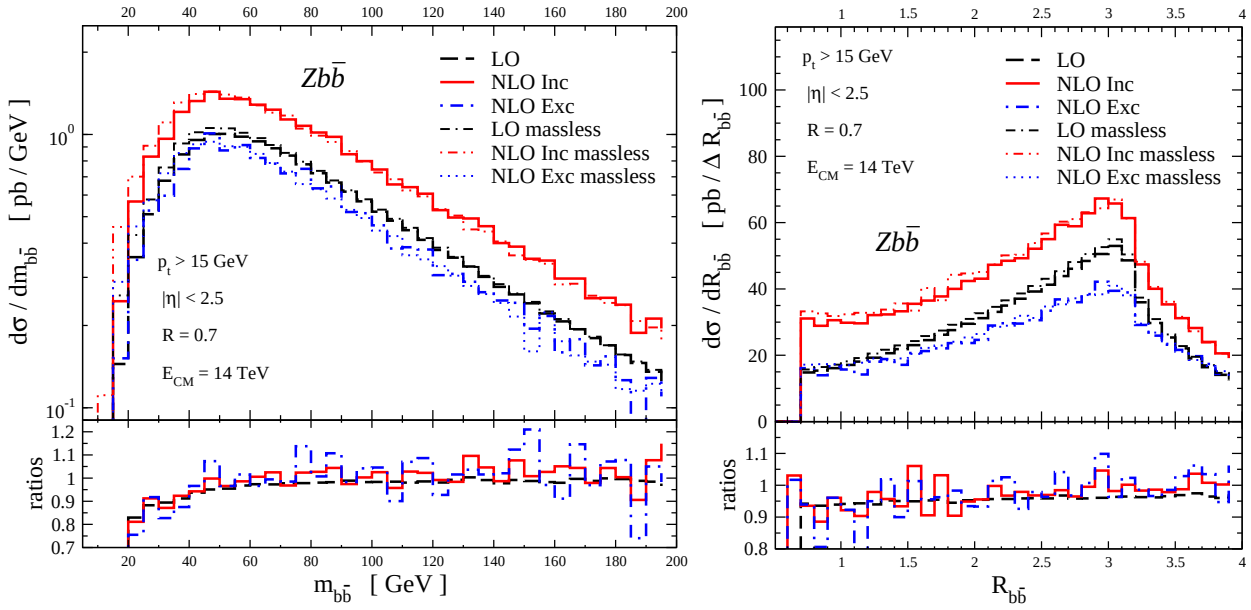

FIG. 16: LO (black), NLO *inclusive* (red) and NLO *exclusive* (blue) $m_{b\bar{b}}$ (left hand side) and $R_{b\bar{b}}$ (right hand side) distributions for $Zb\bar{b}$ production derived from our calculation with $m_b \neq 0$ (LO: dashed, NLO *inclusive*: solid, NLO *exclusive*: dash-dotted) and from MCFM with $m_b = 0$ (LO: double-dashed/dotted, NLO *inclusive*: dashed/double-dotted, NLO *exclusive*: dotted). The lower window shows the ratio of the distributions for massive and massless b quarks, $d\sigma(m_b \neq 0)/d\sigma(m_b = 0)$ (LO: dashed, NLO *inclusive*: solid, NLO *exclusive*: dash-dotted).

hep-ph/0409345.

[27] J. M. Campbell, R. K. Ellis, F. Maltoni, and S. Willenbrock, Phys. Rev. **D69**, 074021 (2004), hep-ph/0312024.

[28] J. Campbell, R. K. Ellis, F. Maltoni, and S. Willenbrock, Phys. Rev. **D73**, 054007 (2006), hep-ph/0510362.

[29] J. Campbell, R. K. Ellis, F. Maltoni, and S. Willenbrock, Phys. Rev. **D75**, 054015 (2007), hep-ph/0611348.

[30] Z. Bern, L. J. Dixon, and D. A. Kosower, Nucl. Phys. **B513**, 3 (1998), hep-ph/9708239.

[31] Z. Bern, L. J. Dixon, D. A. Kosower, and S. Weinzierl, Nucl. Phys. **B489**, 3 (1997), hep-ph/9610370.

[32] R. K. Ellis and S. Veseli, Phys. Rev. **D60**, 011501 (1999), hep-ph/9810489.

[33] J. M. Campbell and R. K. Ellis, Phys. Rev. **D62**, 114012 (2000), hep-ph/0006304.

[34] J. Campbell and R. K. Ellis, Phys. Rev. **D65**, 113007 (2002), hep-ph/0202176.

[35] J. Campbell, R. K. Ellis, and D. L. Rainwater, Phys. Rev. **D68**, 094021 (2003), hep-ph/0308195.

[36] F. Febres Cordero, L. Reina, and D. Wackeroth, Phys. Rev. **D74**, 034007 (2006), hep-ph/0606102.

[37] F. Febres Cordero, L. Reina, and D. Wackeroth, Phys. Rev. **D78**, 074014 (2008), arXiv:0806.0808 [hep-ph].

[38] F. Febres Cordero (2008), arXiv:0809.3829 [hep-ph].

[39] J. M. Campbell et al. (2004), hep-ph/0405302.

[40] K. A. Assamagan et al. (Higgs Working Group) (2004), hep-ph/0406152.

[41] M. Krämer, Nucl. Phys. Proc. Suppl. **135**, 66 (2004), hep-ph/0407080.

[42] J. M. Campbell, R. Frederix, F. Maltoni, and F. Tramontano (2009), arXiv:0903.0005 [hep-ph].

[43] J. Campbell, R. K. Ellis, F. Febres Cordero, F. Maltoni, L. Reina, D. Wackeroth, and S. Willenbrock, Phys. Rev. **D79**, 034023 (2009), arXiv:0809.3003 [hep-ph].

[44] J. Campbell, R. K. Ellis, F. Febres Cordero, F. Maltoni, L. Reina, D. Wackeroth, and S. Willenbrock (2009), in preparation.

[45] J. Campbell and R. K. Ellis, webpage: mcfm.fnal.gov.

[46] H. L. Lai et al. (CTEQ), Eur. Phys. J. **C12**, 375 (2000), hep-ph/9903282.

[47] S. Catani, Y. L. Dokshitzer, and B. R. Webber, Phys. Lett. **B285**, 291 (1992).

[48] S. Catani, Y. L. Dokshitzer, M. H. Seymour, and B. R. Webber, Nucl. Phys. **B406**, 187 (1993).

[49] S. D. Ellis and D. E. Soper, Phys. Rev. **D48**, 3160 (1993), hep-ph/9305266.

[50] W. B. Kilgore and W. T. Giele, Phys. Rev. **D55**, 7183 (1997), hep-ph/9610433.